RSC Advances

This article can be cited before page numbers have been issued, to do this please use: E. Y. L. Teo, H. N. Lim, R. Jose and K. F. Chong, *RSC Adv.*, 2015, DOI: 10.1039/C5RA02578H.

ROYAL SOCIETY OF CHEMISTRY

www.rsc.org/advances

View Article Online
DOI: 10.1039/C5RA02578H

Aminopyrene Functionalized Reduced Graphene Oxide as Supercapacitor Electrode

Ellie Yi Lih Teo [a], Hong Ngee Lim [b], Rajan Jose [a], Kwok Feng Chong [a,*]

[a] Faculty of Industrial Sciences & Technology, Universiti Malaysia Pahang, Lebuhraya Tun Razak, 26300 Gambang, Kuantan, Pahang Darul Makmur, Malaysia

[b] Department of Chemistry, Faculty of Science, Universiti Putra Malaysia, 43400 UPM Serdang, Selangor, Malaysia.

*Author for correspondence: (email: ckfeng@ump.edu.my; Tel.: +609 5492403; Fax: +609 5492766)

ABSTRACT In this work, we report on the structural and electrochemical properties of aminopyrene functionalized reduced graphene oxide (Ap-rGO) for its suitability as supercapacitor electrode. The Ap-rGO is prepared by sonicating a suspension of rGO with aminopyrene and the filtered sediment is subjected by spectroscopy studies and electrochemical studies. Spectroscopy studies reveal the successful functionalization of aminopyrene onto Ap-rGO through π–π interaction. Electrochemical analyses of Ap-rGO show substantial increase in specific capacitance for Ap-rGO (160 F/g at 5 mV/s) compared to the non-functionalized rGO (118 F/g at 5 mV/s). The enhancement is shown to be the

View Article Online
DOI: 10.1039/C5RA02578H

pseudocapacitance arising from the electron donating effect of amine group and the electron accepting effect of rGO, which enable facile electron transfer between surface-bound amine group and rGO. The Ap-rGO has desirable charge storage properties such as low series resistance (0.4 Ω) and superior cycling stability (85% after 5000 cycles). Furthermore, the Ap-rGO has 1.5 fold higher energy density than the non-functionalized rGO electrode, thereby making it suitable as a deployable supercapacitor electrode.

KEYWORDS: aminopyrene; graphene; pseudocapacitance; redox; supercapacitor

1. INTRODUCTION

A modern technological society demands the storage of energy on a large scale. In the context of energy storage, high performance energy storage device is expected to supply energy at fast rate. Conventional energy storage device such as capacitor and battery could not fulfill the increasing technological demands as the capacitor is limited by low energy density whereas battery is limited by low power density. In this context, supercapacitors are promising energy storage device with higher energy density (≥5 Wh/kg) than capacitors and delivers energy at higher rate (≥10 kW/kg) than batteries. A supercapacitor could be fully charged or discharged in seconds; therefore attracting worldwide research interests due to diverse applications ranging from household electronic products to emergency doors in Airbus A380 planes.[1-2] There are two types of charge storage mechanisms in supercapacitor: electrochemical double layer capacitance (EDLC) and pseudocapacitance. In EDLC, electric energy is stored through the accumulation of electric charges at an electrode/electrolyte interface, without faradaic reaction. Therefore, EDLC are highly stable as they do not involve any phase changes during charge storage process. Carbon such as activated carbon and carbon nanotubes are popular choice for EDLC electrode.[1-2] On the other hand, charge storage mechanism of pseudocapacitance is based on faradaic process where a redox reaction occurs at the electrode surface.

View Article Online
DOI: 10.1039/C5RA02578H

Metal oxides and conducting polymers are the common electrode materials with large pseudocapacitance effect.[3-6] Pseudocapacitance is generally higher than EDLC due to faradaic process, however, at the expense of the long term stability of the electrode. Therefore, the integration of both EDLC and pseudocapacitance in a supercapacitor could be a solution to fabricate high performance supercapacitor with long term stability.

Since its discovery in 2004, graphene is gaining interest as the supercapacitor electrode owing to its good electrical conductivity, chemical inertness, excellent mechanical property and high specific surface area.[7-10] The intrinsic capacitance of graphene was reported to be 21 $\mu F/cm^2$, the highest value among all carbon-based materials.[11] Ruoff *et al.* demonstrated that the reduced graphene oxides (rGO) exhibit EDLC with specific capacitance values of 135 and 99 F/g in aqueous and organic electrolytes, respectively.[12] In order to enhance the capacity of graphene as high performance supercapacitor, various graphene composites such as metal oxides/graphene and polymer/graphene is proposed to incorporate pseudocapacitance with EDLC of graphene.[13-17] In addition to graphene composites, organically functionalized graphene is also tested as the supercapacitors electrode with pseudocapacitance. Pyrenecarboxylic acid functionalized graphene shows dramatic increase in the specific capacitance values.[18-19] However, to the best of our knowledge, there has been no report on the aminopyrene functionalized graphene as supercapacitor electrode. Amine functional group in aminopyrene is an electron donating group which could donate electrons to graphene, an electron acceptor which could accept multiple electrons due to its 2D expanse network. Such electron transfer is expected to produce charge differential that yields pseudocapacitance. Herein, we report the electrochemical properties of aminopyrene functionalized reduced graphene oxide (Ap-rGO) and the results are compared with the nonfunctionalized rGO.

2. EXPERIMENTAL

2.1 Materials and reagents

View Article Online
DOI: 10.1039/C5RA02578H

Graphite powder (fine powder, extra pure) as the starting material was obtained from Merck. Concentrated hydrochloric acid (HCl, 37 %), hydrogen peroxide (H_2O_2, 30 wt%), concentrated sulphuric acid (H_2SO_4, 99.9 %), potassium permanganate ($KMnO_4$), phosphorus pentoxide (P_2O_5), potassium persulfate ($K_2S_2O_8$), hydrazine monohydrate (N_2H_2, 35 %) and 1-aminopyrene (97 %) were obtained from Sigma-Aldrich.

2.2 Sample preparation

The graphene oxide (GO) was prepared using modified Hummers' method.[20] Briefly, graphite powder (4.0 g) was added into a mixture of concentrated H_2SO_4 (60 mL) and $K_2S_2O_8$ (6.0 g). The mixture was stirred and maintained at 80 °C for 6 h before cooling to room temperature. It was then diluted with deionized water (2 L), filtered and washed until the filtrate became neutral in pH. The product (pre-oxidized graphite) was collected and dried overnight in vacuum. Then, it was further oxidized by adding it into concentrated H_2SO_4 (300 mL) at 0 °C. $KMnO_4$ (35.0 g) was gradually added into the mixture under stirring and kept at 35 °C for 4 h. The mixture was diluted with deionized water (1 L) followed by the addition of H_2O_2 (100 mL). The mixture was filtered, washed with 1:10 HCl (5 L) and dried overnight in vacuum to obtain the dry graphite oxide (GO). The GO was exfoliated by sonicating graphite oxide dispersion (2 mg/mL) for 30 min. Unexfoliated GO was removed by centrifugation at 10000 rpm for 10 min. A homogeneous yellow brown supernatant was obtained as GO dispersion. The GO reduction was performed by adding N_2H_4 (1.2 mL) into a GO dispersion (50 mL) and the mixture was refluxed at 95 °C for 24 h. Dried reduced GO (rGO) was obtained by vacuum filtration, washed with deionized water and dried overnight in vacuum. Aminopyrene functionalized reduced graphene oxide (Ap-rGO) was obtained by sonicating rGO (10 mg) and 1-aminopyrene (10 mg) in ethanolic solution for 1 h, followed by overnight stirring at room temperature. Excessive 1-aminopyrene was used for the complete functionalization of the rGO (Supplementary Data Figure S1). The dried Ap-rGO was collected after overnight drying in vacuum. The amount of aminopyrene successfully functionalized onto rGO was quantified by calibration curve of series of 1-aminopyrene solutions with peak

View Article Online
DOI: 10.1039/C5RA02578H

absorbance at 241 nm (Supplementary Data Figure S2). It was calculated that 5 wt.% of aminopyrene was successfully functionalized in Ap-rGO.

2.3 Characterization

UV-Vis measurements were conducted by dispersing GO, rGO, Ap-rGO in deionized water at 0.1 mg/mL concentration and they were scanned from 200 to 400 nm using Thermo Scientific spectrophotometer. FTIR measurements were performed in the frequency of 400 to 4000 cm^{-1} with Perkin Elmer Spectrum 100 spectrophotometer. Fluorescence emission spectra were recorded using Tecan Infinite 200 Pro with excitation wavelength of 356 nm. The morphology of Ap-rGO was observed under the JEOL 1525 field emission scanning electron microscope (FESEM). Raman spectra were measured with Renishaw in-Via Raman microscope with 532 nm laser.

2.4 Electrode preparation and electrochemical studies

The electrodes were prepared by brush coating homogenous mixture (sample, carbon black and PVDF in the ratio of 80:15:5) onto a nickel foam. Nickel foam was used as the current collector as it possesses high conductivity, 3D open-pore structure as well as high specific surface area.[21-22] The mass load of active material on each electrode was 5-10 mg and all the calculated capacitance values were normalized against electrode mass. Two sample-coated electrodes were separated by a glass microfiber membrane pre-soaked in 6 M KOH electrolyte. The setup was sandwiched by two stainless steel plates, connected to an Autolab PGSTAT M101 potentiostat/galvanostat for electrochemical studies. The cyclic voltammetry (CV) was performed at potential between 0 V and 1 V at scan rates ranging from 5 mV/s to 100 mV/s. Galvanostatic charge discharge measurements were conducted over potential window from 0 to 1 V at different current densities (from 0.1 A/g to 1.0 A/g). Electrochemical impedance spectroscopy (EIS) results were obtained at open circuit potential from frequency 500 kHz to 10 mHz.

3. RESULTS AND DISCUSSION

View Article Online
DOI: 10.1039/C5RA02578H

Figure 1 shows the UV spectra for GO, rGO and Ap-rGO. The GO exhibits a characteristic peak at 230 nm which could be attributed to the π-π* transition of the C=C bond. The π-conjugation network is restored during reduction process and the corresponding absorption peak is red-shifted to 266 nm, as seen in the absorption spectrum of rGO.[23] Apart from π-π* transition at 266 nm, two additional absorption peaks could be observed for Ap-rGO at 241 nm and 353 nm, possibly due to the electronic transition within aminopyrene.[24] The absorption of Ap-rGO at 353 nm was further tested with fluorescence spectroscopy and it shows the fluorescence intensity at 405 nm is significantly quenched on Ap-rGO as compared to that obtained on pure 1-aminopyrene (See Supplementary Data Figure S3). The close proximity between aminopyrene and rGO in Ap-rGO structure due to the planar configuration of aminopyrene enables effective electron transfer between aminopyrene and rGO, thus suggesting Ap-rGO as a superior electrode for electrochemical applications.

The functional groups present in the samples were tested by FTIR (Figure 2). There are several peaks observed in the spectrum of GO; the broad peak at 3402 cm^{-1} is attributed to the stretching vibration of O–H functional group, the peak at 1740 cm^{-1} is due to the C=O functional group and the peak at 1052 cm^{-1} is attributed to the C–O stretching vibrations. A peak is also detected at 1631 cm^{-1} which is due to the skeletal vibrations of unoxidized graphitic domain.[25] After reduction, the intensities of the oxygen-related peaks are significantly decreased. This signifies that the reduction process successfully removes most of the oxygen-containing functional groups in GO.[26-27] The functionalization of aminopyrene on rGO can be visibly seen in the spectrum of Ap-rGO. N–H stretching and bending could be seen at 3421 cm^{-1} and 1563 cm^{-1}, respectively. In addition, absorption bands at 1194 cm^{-1} and 834 cm^{-1} could be attributed to the C-N stretching and N-H wagging, respectively. The FTIR findings complement the UV results to suggest the successful aminopyrene functionalization in Ap-rGO.

Raman spectroscopy technique is a powerful technique used to probe the structural information of carbon-based materials including graphene. Figure 3 shows the Raman spectra for rGO and Ap-rGO. The laser excitation (512 nm) causes the Stokes phonon energy shift which results in the appearance of

View Article Online
DOI: 10.1039/C5RA02578H

two prominent peaks (D-band and G-band) of graphene in both rGO and Ap-rGO.[28] The defects present and the sp^3 bonding in the material is associated with the D-band.[29] Meanwhile, the G-band represents the graphitic material that is present within the structure.[30] In this work, the ratios of I_D/I_G for rGO and Ap-rGO were computed to be 1.11 and 0.97, respectively. The lower I_D/I_G ratio for Ap-rGO could indicate fewer defect sites present in the sample and this is in agreement with the study by Li *et al*. which stated that the pyrene derivatives are able to act as a nanographene to repair the defects present.[31]

The representative CV curves for rGO and Ap-rGO electrodes in 6 M KOH are shown in Figure 4a. The rGO electrode shows desirable charge propagation within the sample as shown in the rectangular shape in CV which is a typical behavior for EDLC.[32] In addition to the broad rectangular shape in CV, a pair of redox peaks can be observed for Ap-rGO electrode. The presence of reversible redox peaks (0.47 V/0.35 V) shows that Ap-rGO demonstrates the pseudocapacitve behavior in addition to the EDLC presented by rGO. The specific capacitance values are calculated by integrating over the full CV curve for the average value and are summarized in Figure 4b.[33] Clearly seen that both rGO electrode and Ap-rGO electrode show decreasing trend in the specific capacitance values with increasing scan rate, possibly due to the inability of the electrolyte ions to penetrate into the electrode inner surface at high scan rates. However, it is noteworthy to highlight the enhanced specific capacitance attained on Ap-rGO electrode. The highest specific capacitance value attained on Ap-rGO electrode is 160 F/g at 5 mV/s, which is about 1.5 times higher as compared to that obtained on rGO electrode (118 F/g at 5 mV/s). The specific capacitance enhancement in Ap-rGO electrode could be attributed to the faradaic redox reaction in Ap-rGO that could contribute to the pseudocapacitance of the electrode. The electron donating effect of aminopyrene could enable efficient electron transfer into the large 2D expanse of graphene network as electron accepting group. Furthermore, electron transfer is also facilitated through the planar configuration of aminopyrene that brings amine group to the close proximity of rGO surface. Apart from redox reaction, the enhanced specific capacitance of Ap-rGO electrode could be related to the improved surface wettability (See Supplementary Data Figure S4). The inclusion of amine group in Ap-rGO could reduce the hydrophobicity nature of the rGO, thus enhancing aqueous electrolyte ions

View Article Online
DOI: 10.1039/C5RA02578H

diffusion within Ap-rGO electrode. However, the specific capacitance enhancement for Ap-rGO is decreasing with increasing scan rate, where the specific capacitance value for Ap-rGO electrode (98 F/g) is very similar to those obtained on rGO electrode (95 F/g) at high scan rate (100 mV/s). It could be caused by the blockage of the interlayer spacing by aminopyrene in Ap-rGO, thus reducing its accessibility to electrolyte ions at high scan rate, which causes lower ions absorption and lower capacitance.

To assess the feasibility of Ap-rGO electrode in the application of supercapacitor, galvanostatic charge-discharge was performed at various current densities (Figure 5). The non-linearity of the discharge curves indicates the presence of pseudocapacitance in Ap-rGO electrode. Similar as CV observation, discharge curves of Ap-rGO electrode show shoulder at ca. 0.48 V, which indicates redox reaction. The shape of the charge-discharge curves is independent of the current density, thereby indicating that the Ap-rGO electrode is suitable for the application of supercapacitor. Contrary to the non-linearity of the discharge curves for Ap-rGO electrode, rGO electrode shows pure EDLC with linear discharge curve (Figure 5 inset). Figure 6 shows the Nyquist plots for both rGO electrode and Ap-rGO electrode. Both of them show similar trend: a semicircle at high frequency followed by near 90° linear line at low frequency region. The inset picture depicts the clear semicircle with intercept at the *x*-axis. The intercept represents the equivalent series resistance (ESR) of the electrode and it is approximated to be ca. 0.6 Ω and ca. 0.4 Ω for rGO electrode and Ap-rGO electrode, respectively. The relatively lower ESR value for Ap-rGO electrode is expected, due to the improved surface wettability that facilitates access of the electrolyte ions to the electrode surface and shortens the ionic diffusion time. The semicircle could be extrapolated to the *x*-axis and its diameter is related to the charge transfer resistance (R_{ct}). Contrary to ESR, R_{ct} value for Ap-rGO electrode (1.4 Ω) is higher than that obtained on rGO electrode (0.7 Ω), probably due to the aminopyrene functional group that could impede electron transfer to the electrode. The near 90° linear line at low frequency region is associated with interfacial diffusive resistance and it is also termed as Warburg resistance.[34] The near 90° linear line can be related to superior capacitive behavior for both rGO electrode and Ap-rGO electrode. In comparison, the

View Article Online
DOI: 10.1039/C5RA02578H

Warburg line for Ap-rGO electrode is shorter than that for rGO electrode, which is an indication that the Ap-rGO electrode has shorter ions diffusion path that may be due to the improved surface wettability.

The rate capability of the electrodes was studied using the complex Bode plots, according to the following equations:

$$C'(\omega) = \frac{-Z''(\omega)}{\omega\,|Z(\omega)\,|^2} \quad (1)$$

$$C''(\omega) = \frac{-Z'(\omega)}{\omega\,|Z(\omega)\,|^2} \quad (2)$$

where C' represents the real part of the cell capacitance and C'' is the imaginary part related to the losses in the charge storage process leading to an energy dissipation.[35] $Z'(\omega)$ and $Z''(\omega)$ are the respective real and imaginary parts of the complex impedance. ω is the angular frequency and it is given by $\omega = 2\pi f$. The C' plots in Figure 7a shows similar trend as the results obtained from CV measurements, where higher specific capacitance was attained on Ap-rGO electrode (98 mF) as compared to that obtained on rGO electrode (42 mF). On the other hand, the C'' plots (Figure 7b) can be used to calculate the relaxation time constant (τ_0) with the equation $\tau_0 = 1/(2\pi f_0)$, where f_0 is the maximum frequency of the peak. It also can be defined as the minimum time required to discharge all of the energy with more than 50% efficiency.[36] The maximum peak in C'' plots for Ap-rGO electrode shifts towards lower frequency because of the increased capacitance.[37] The τ_0 obtained for Ap-rGO electrode (0.88 s) is higher than that obtained on rGO electrode (0.05 s). However, it is still maintained at a reasonable value as compared to the reported values for other functionalized graphene electrodes such as graphene/polyaniline electrode (0.60 s) and graphene/$Ni(OH)_2$ (0.80 s).[38-39]

Cycling stability is an important parameter for the actual practical usage of a supercapacitor. The cycling stability of the Ap-rGO electrode was evaluated by performing constant charge-discharge at current density of 0.5 A/g for 5000 cycles (Figure 8). Interestingly, Ap-rGO electrode with pseudocapacitive behavior is able to maintain its capacitance at ca. 85% after 5000 charge-discharge cycles and only little variation could be found in the charge-discharge curve at 5000th cycle (Figure 8 inset). It suggests the suitability of Ap-rGO electrode for supercapacitor application, even with

View Article Online
DOI: 10.1039/C5RA02578H

pseudocapacitive behavior. The energy and power performance of Ap-rGO electrode is evaluated in Ragone plot (Figure 9). It can be observed that the energy density for Ap-rGO electrode is about 1.5 fold higher than rGO electrode, with highest energy density attained on Ap-rGO electrode as 5.6 Wh/kg.

4. CONCLUSIONS

We have demonstrated the Ap-rGO can be a superior electrode material for supercapacitor application. The role of aminopyrene in Ap-rGO in enhancing the specific capacitance could be highlighted in two aspects: 1) pseudocapacitive behavior of amine group, and 2) hydrophilic property of amine group that contributes to improved electrolyte ions diffusion. Interestingly, the inclusion of pseudocapacitive aminopyrene into rGO network increases the specific capacitance (1.5 folds higher than the rGO), without compromising the cycling stability of the electrode. Moreover, low ESR value of Ap-rGO electrode suggests low power consumption, which will lead to efficient energy storage system. Such excellent charge storage properties render Ap-rGO as promising electrode material for supercapacitor application.

ACKNOWLEDGEMENT

KF Chong and co-workers would like to acknowledge the funding from the Ministry of Education Malaysia in the form of MTUN-COE (RDU121213) and Ministry of Science, Technology and Innovation in the form of eScienceFund (06-01-16-SF0094).

REFERENCE

1. M. Winter and R. J. Brodd, *Chem. Rev*., 2004, **104**, 4245.
2. P. Simon and Y. Gogotsi, *Nature Mat*., 2008, **7**, 845.
3. S. Vijayakumar, S. Nagamuthu and G. Muralidharan, *ACS Appl. Mater. Inter*., 2013, **5**, 2188.
4. Y. Lei, J. Li, Y. Wang, L. Gu, Y. Chang, H. Yuan and D. Xiao, *ACS Appl. Mater. Inter*., 2014, **6**, 1773.
5. S. Cho, K. Shin and J. Jang, *ACS Appl. Mater. Inter*., 2013, **5**, 9186.
6. Y. Weng and N. Wu, *J. Power Sources*, 2013, **238**, 69.
7. A. K. Geim and K. Novoselov, *Nat. Mat*., 2007, **6**, 183.
8. Y. Zhu, S. Murali, W. Cai, X. Li, J. W. Suk. J. R. Potts and R. S. Ruoff, *Adv. Mater*., 2010, **22**, 3906.

View Article Online
DOI: 10.1039/C5RA02578H

9. S. Park, J. An, R. D. Piner, I. Jung, D. Yang, A. Velamakanni, S. T. Nguyen and R. S. Ruoff, *Chem. Mater*., 2008, **20**, 6592.
10. S. Stankovich, D. A. Dikin, G. H. B. Dommett, K. M. Kolhlhaas, E. J. Zimney, E. A.Stach, R. D. Piner, S. T. Nguyen and R. S. Ruoff, *Nat. Lett*., 2006, **442**, 282.
11. J. Xia, F. Chen, J. Li and N. Tao, *Nat. Nanotechnol*., 2009, **4**, 505.
12. M. D. Stoller, S. Park, Y. Zhu, J. An and R. S. Ruoff, *Nano Lett*., 2008, **8**, 3498.
13. H. Chen, S. Zhou and L. Wu, *ACS Appl. Inter*., 2014, **6**, 8621.
14. L. Ma, X. Shen, H. Zhou, Z. Ji, K. Chen and G. Zhu, *Chem. Eng. J*., 2015, **262**, 980.
15. N. B. Trung, T. V. Tam, H. R. Kim, S. H. Hur, E. J. Kim and W. M. Choi, *Chem. Eng. J*., 2014, **255**, 89.
16. T. Fan S. Tong, W. Zeng, Q. Niu, Y. Liu, C. Kao, J. Liu, W. Huang, Y. Min and A. J. Epstein, *Synthetic Met*., 2015, **199**, 79.
17. W. K. Chee, H. N. Lim, I. Harrison, K. F. Chong, Z. Zainal, C. H. Ng and N. M. Huang, *Electrochim. Acta*, 2015, **157**, 88.
18. S. Ghosh, X. An, R. Shah, D. Rawat, B. Dave, S. Kar and S. Talapatra, *J. Phys. Chem. C*, 2012, **116**, 20688.
19. X. An, T. Simmons, R. Shah, C. Wolfe, K.M. Lewis, M. Washington, S.K. Nayak, S. Talapatra and S. Kar, *Nano Lett*., 2010, **10**, 4295.
20. W. S. Hummers Jr. and R. E. Offeman, *J. Am. Chem. Soc*.,1958, **80**, 1339.
21. Y. Wang, Y. Zhao and C. Xu, *J. Solid State Electrochem*., 2012, **16**, 829.
22. G. Yang, C. Xu and H. Lin, *Chem. Commun*., 2008, **48**, 6537.
23. E. Choi, T. H. Han, J. Hong, J. E. Kim, S. H. Lee, H. W. Kim and S. O. Kim, *J. Mater. Chem*., 2010, **20**, 1907.
24. L. Luo, Z. Zhang, Y. Ding, D. Deng, X. Zhu and Z. Wang, *Nanoscale,* 2013, **5**, 5833.
25. Y. Xu, H. Bai, G. Lu, C. Li and G. Shi, *J. Am. Chem. Soc*., 2008, **130**, 5856.
26. P. Zhu, M. Shen, S. Xiao and D. Zhang, *Physica B*, 2011, **406**, 498.
27. J. Liu, R. Wang, L. Cui, J. Tang, Z. Liu, Q. Kong, W. Yang and J. Gooding, *J. Phys. Chem. C*., 2012, **116**, 17939.
28. L. Li, J. Zhang, Y. Liu, W. Zhang, H. Yang, J. Chen and Q. Xu, *ACS Sustainable Chem. Eng*., 2013, **1**, 527.
29. D. Liu, L. Yang, J. S. Huang, Q. H. Guo and T. Y. You, *RSC Adv*., 2014, **4**, 13733.
30. D. N. H. Tran, S. Kabiri and D. Losic, *Carbon*, 2014, **76**, 193.
31. L. Li, X. Zheng, J. Wang, Q. Sun and Q. Xu, *ACS Sustainable Chem. Eng*., 2013, **1**, 144.
32. O. Gilbert, B. E. Kumara Swamy, U. Chandra and B. S. Sherigara, *Int. J. Electrochem. Sci*., 2009, **4**, 582.
33. M. D. Stoller and R. S. Ruoff, *Energy Environ. Sci*., 2010, **3**, 1294.
34. M. Zhi, A. Manivannan, F. Meng and N. Wu, *J. Power Sources,* 2012, **208**, 345.
35. G. P. Pandey, A. C. Rastogi, C. R. Westgate, *J. Power Sources*, 2014, **245**, 857.
36. A. A. Radhiyah, I. I. Misnon, K. F. Chong, M. M. Yusoff, R. Jose, *Electrochim. Acta*, 2013, **113**, 141.
37. P. Sivaraman, A. R. Bhattacharrya, S. P. Mishra, A. P. Thakur, K. Shashidhara and A. B. Samui, *Electrochim. Acta*, 2013, **94**, 182.
38. P. A. Basnayaka, M. K. Ram, E. K. Stefanakos and A. Kumar, *Electrochim. Acta*, 2013, **92**, 376.
39. J. Yan, W. Sun, T. Wei, Q. Zhang, Z. Fan and F. Wei, *J. Mater. Chem*., 2012, **22**, 11494.

View Article Online
DOI: 10.1039/C5RA02578H

View Article Online
DOI: 10.1039/C5RA02578H

Figure caption

Figure 1 UV spectra of GO, rGO and Ap-rGO.

Figure 2 FTIR spectra of GO, rGO and Ap-rGO.

Figure 3 Raman spectra of rGO and Ap-rGO.

Figure 4 (a) Cyclic voltammogram of rGO electrode and Ap-rGO electrode at 20 mV/s in 6 M KOH, (b) Specific capacitance variation as a function of scan rate for rGO electrode and Ap-rGO electrode.

Figure 5 Charge discharge curves of Ap-rGO electrode at various current densities in 6 M KOH, inset shows the charge discharge curve of rGO electrode.

Figure 6 Impedance spectra of rGO electrode and Ap-rGO electrode at open circuit potential in 6 M KOH, inset shows the high frequency region.

Figure 7 Evolution of the (a) real part and (b) imaginary part of the capacitance vs. the frequency for rGO electrode and Ap-rGO electrode.

Figure 8 Stability test for Ap-rGO electrode in 6 M KOH at 0.5 A/g. Inset shows the charge discharge curves at 1^{st} cycle and 5000^{th} cycle.

Figure 9 Ragone plot for rGO electrode and Ap-rGO electrode.

View Article Online
DOI: 10.1039/C5RA02578H

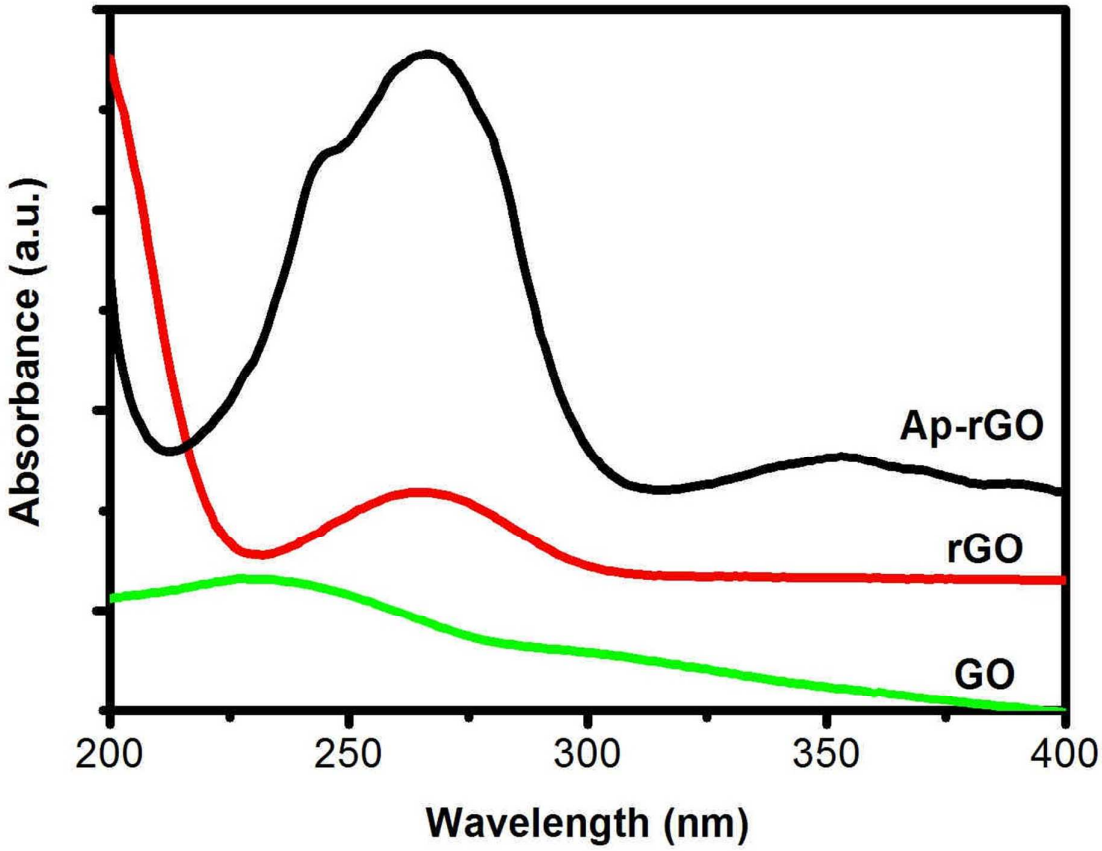

Figure 1

View Article Online
DOI: 10.1039/C5RA02578H

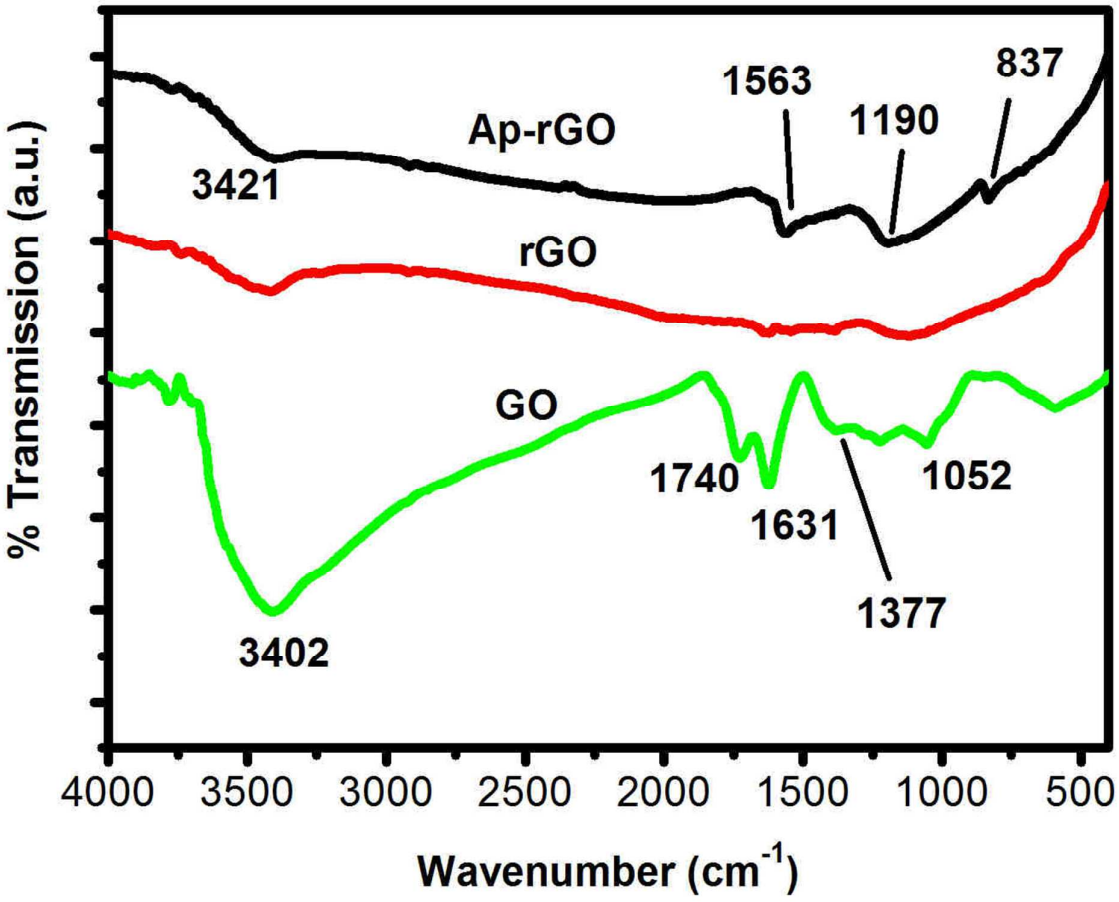

Figure 2

View Article Online
DOI: 10.1039/C5RA02578H

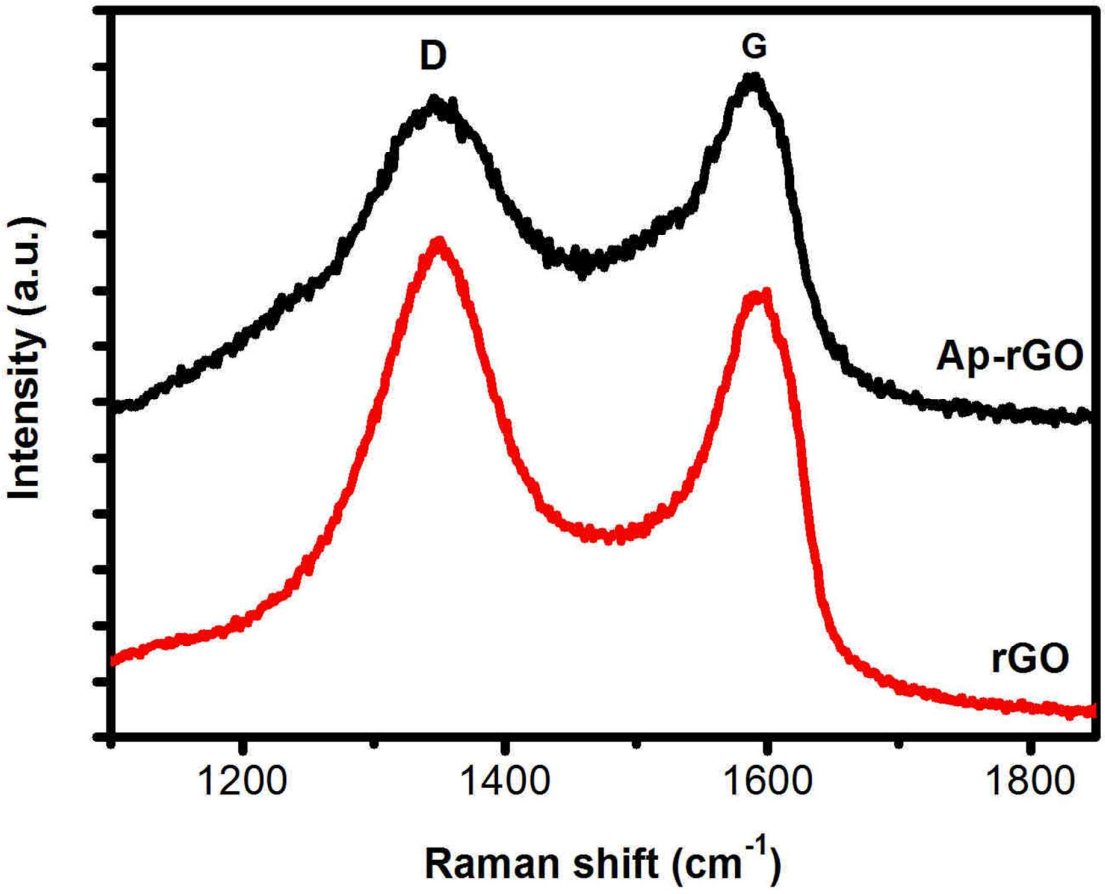

Figure 3

View Article Online
DOI: 10.1039/C5RA02578H

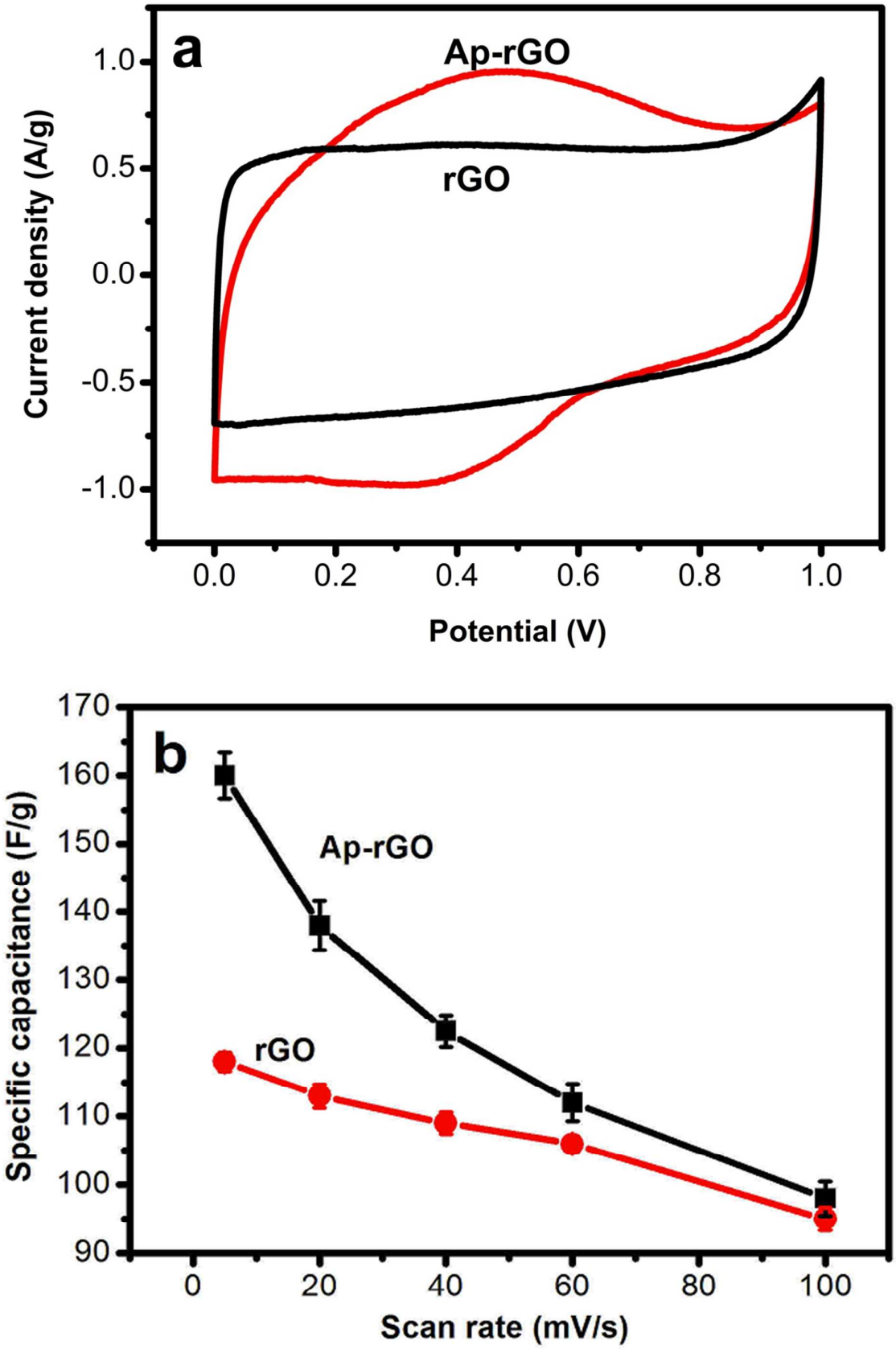

Figure 4

View Article Online
DOI: 10.1039/C5RA02578H

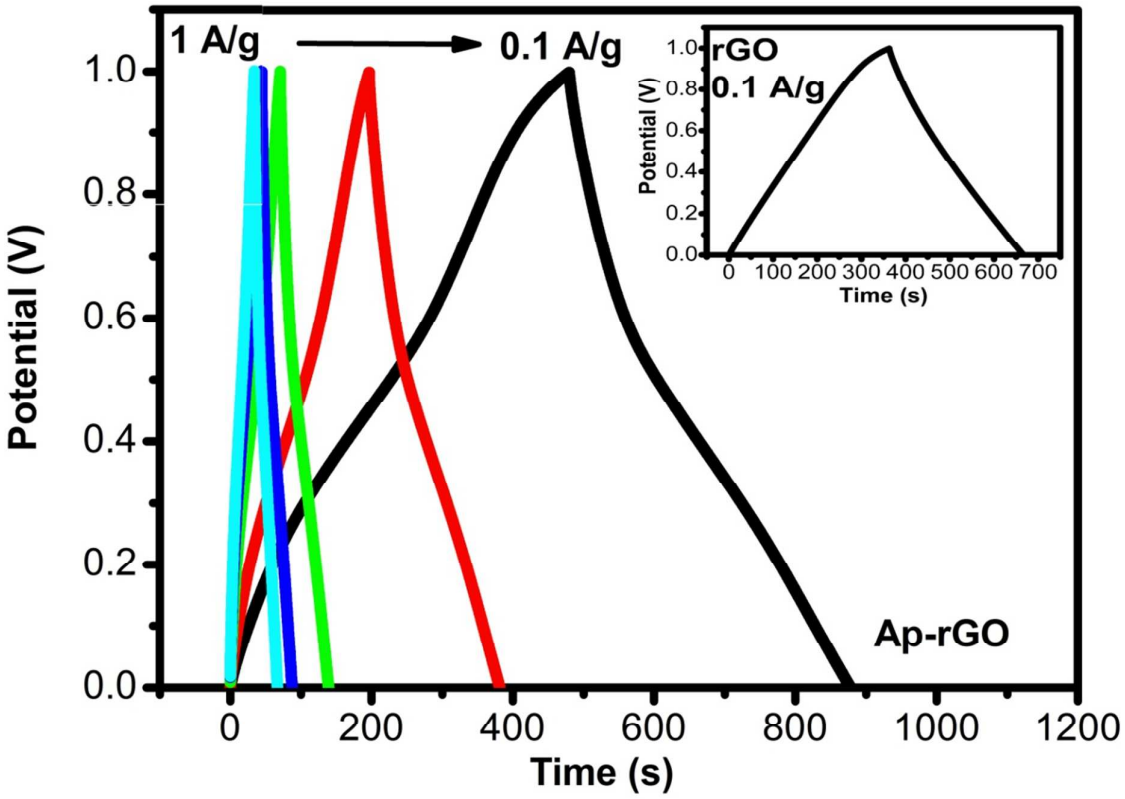

Figure 5

View Article Online
DOI: 10.1039/C5RA02578H

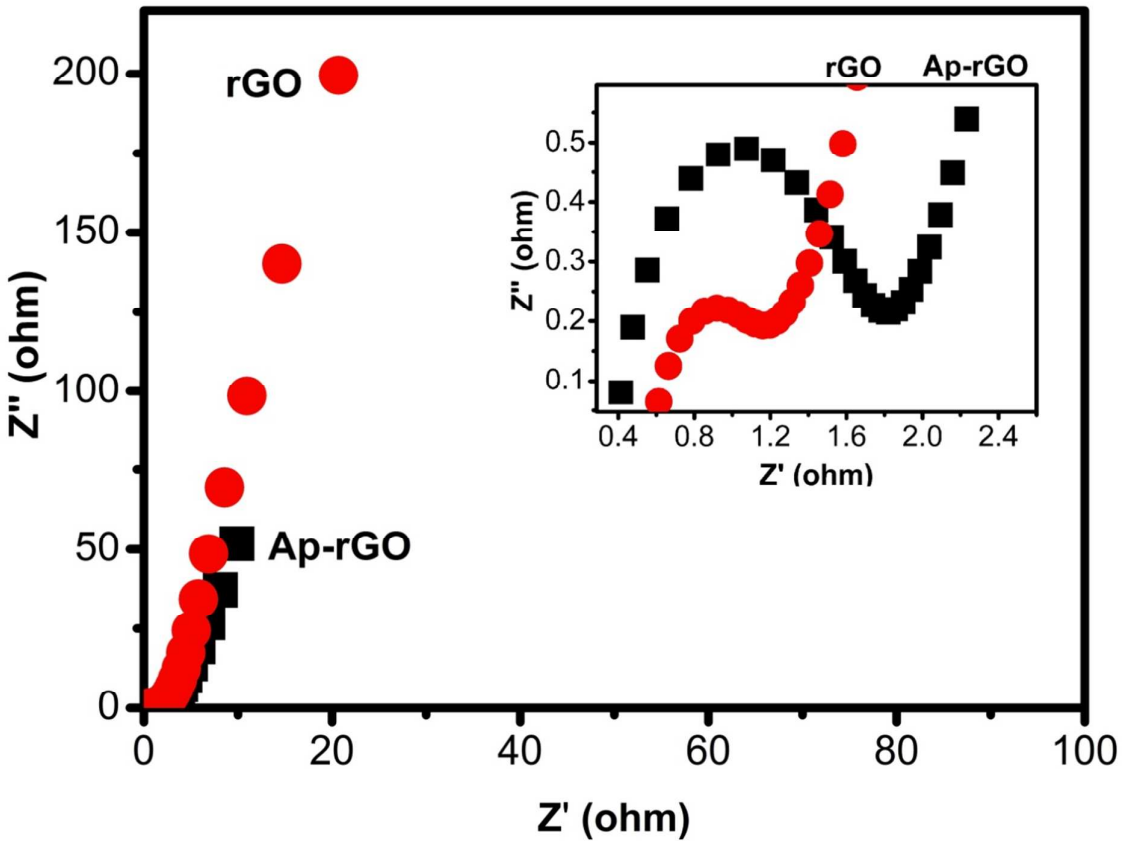

Figure 6

View Article Online
DOI: 10.1039/C5RA02578H

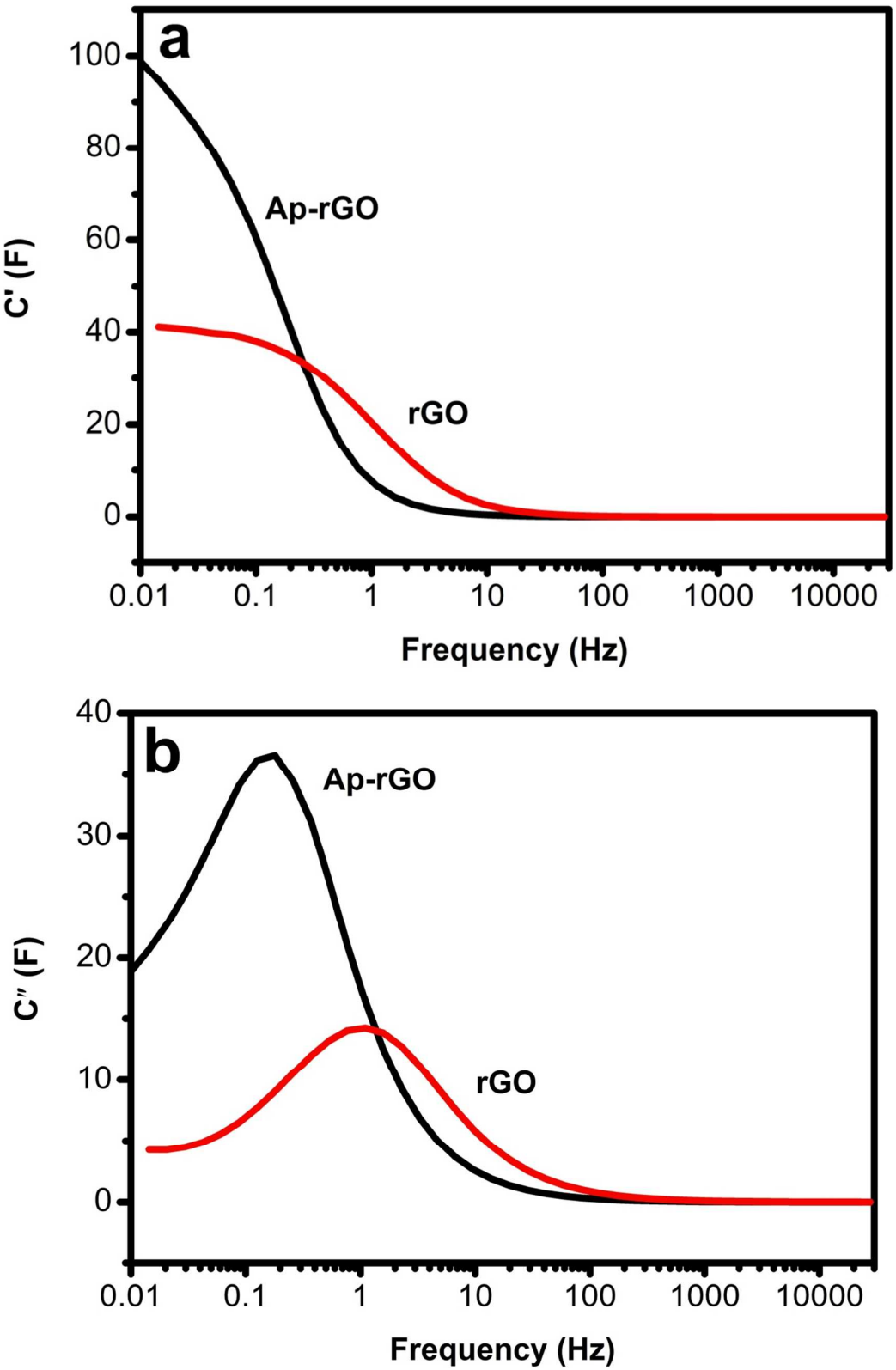

Figure 7

View Article Online
DOI: 10.1039/C5RA02578H

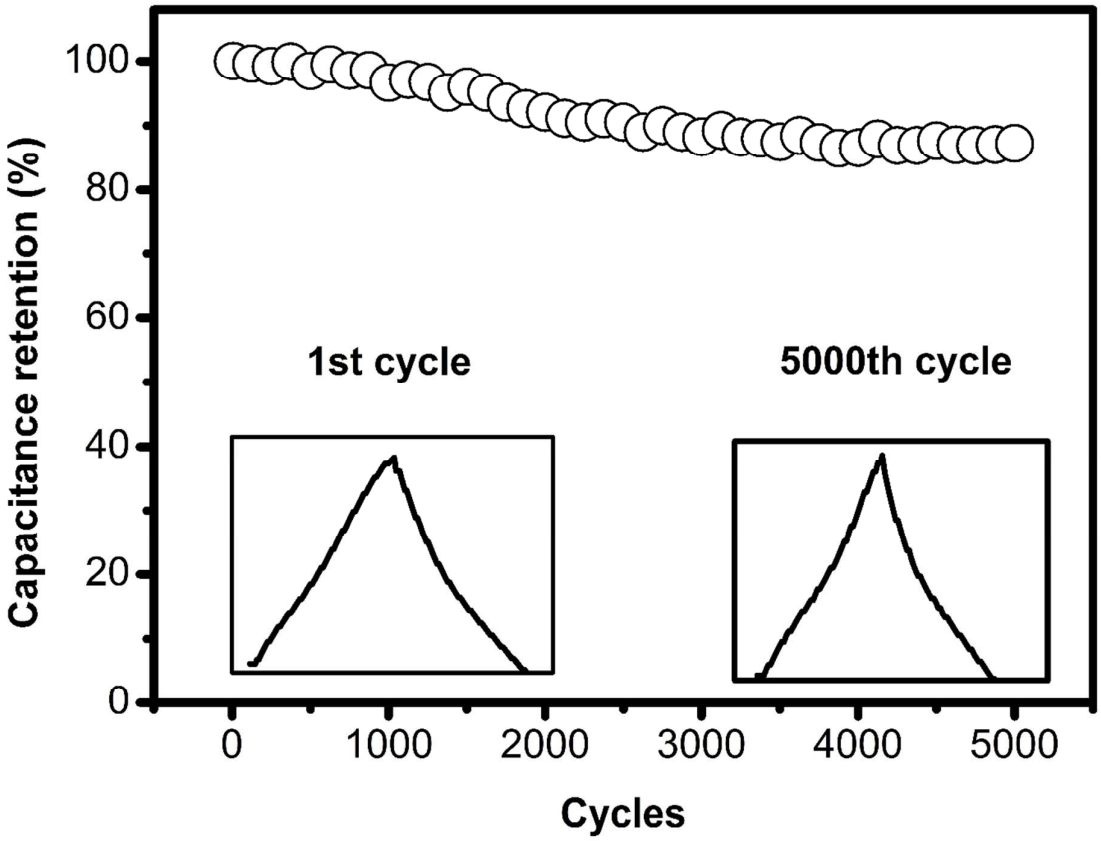

Figure 8

View Article Online
DOI: 10.1039/C5RA02578H

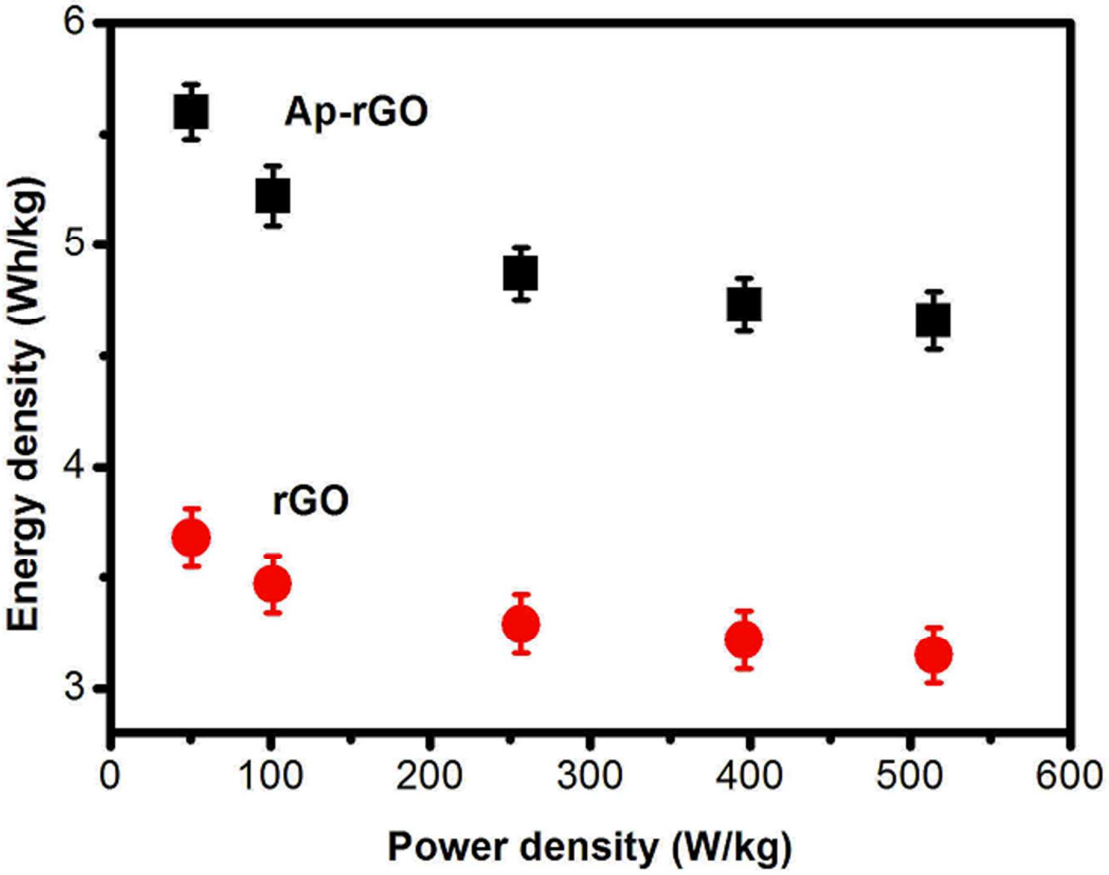

Figure 9